

Modeling Eclipses of the Novalike Variable TT Triangulum

S. R. Warren,¹ A. W. Shafter & J. K. Reed

*Department of Astronomy and Mount Laguna Observatory
San Diego State University
San Diego, CA 92182*

warren@astro.umn.edu, aws@nova.sdsu.edu, jreed@sciences.sdsu.edu

ABSTRACT

Multicolor (*BVRI*) light curves of the eclipsing novalike variable TT Tri are presented. The eclipse profiles are analyzed with a parameter-fitting model that assumes four sources of luminosity: a white dwarf primary star, a main-sequence secondary star, a flared accretion disk with a rim, and a bright spot at the intersection of the mass-transfer stream and the disk periphery. Model parameters include the temperatures of the white dwarf (T_1) and the secondary star (T_2), the radius (R_d) and temperature (T_d) of the disk periphery, the inner disk radius (R_{in}), the disk power-law radial brightness temperature exponent (α) and thickness parameter (h_r), and a bright spot temperature enhancement factor (χ_s).

A grid of model model light curves was computed, covering an extensive range of plausible parameter values. The models were then compared with the mean *BVRI* light curves to determine the optimum values for the fitting parameters and their associated errors. The mass ratio of TT Tri is poorly constrained in our models, but must lie roughly in the range $0.3 \lesssim q (= M_2/M_1) \lesssim 0.9$. Models characterized by mass ratios of $q = 0.3$ ($i = 76.1^\circ$), $q = 0.6$ ($i = 72.6^\circ$), and $q = 0.9$ ($i = 70.4^\circ$) were all capable of providing acceptable fits to the data, although the best fits were achieved for mass ratios near the upper end of the permitted range ($q = 0.6$ and $q = 0.9$). The values of the remaining fitting parameters were found to be insensitive to the adopted mass ratio and rim thickness. The accretion disk was found to extend to $\sim 50 - 60\%$ of the distance to the inner Lagrangian point in all models, but came closer to reaching the tidal limit (as expected for steady-state accretion) in the higher mass ratio models. The same behavior was found for the radial temperature profile of the disk, which increased with mass ratio, becoming more consistent with that expected for steady state accretion in the $q = 0.6$ and $q = 0.9$ models. Models with a truncated inner disk ($R_{in} \gg R_1$) generally resulted in a higher white dwarf

temperature, and a steepening of the disk temperature profile, but were not required to achieve a viable steady-state disk solution. No evidence was found for a luminous bright spot in the system, which is not surprising given the lack of a pre-eclipse “hump” in the light curve.

A total of 22 eclipse timings were measured for the system, which yielded an ephemeris for the times of mid-eclipse given by $JD_{\odot} = 2,453,618.953(3) + 0.1396369(4) E$. A comparison of the observed brightness and color at mid-eclipse with the photometric properties of the best-fitting model suggests that TT Tri lies at a distance of $\sim 400 - 500$ pc.

Subject headings: binaries: eclipsing - novae, cataclysmic variables - stars: dwarf novae - stars: individual (TT Triangulum)

1. Introduction

TT Tri (GR 286, HS0129+2933) is a little-studied cataclysmic variable star, identified originally as an eclipsing binary by Romano (1978a,b) in a sample of eleven variable stars discovered on Schmidt plates of a field near M33. Except for the refined astrometric measurements of Sharov (1992), the star languished in obscurity until it surfaced in the Hamburg Quasar Survey (Hagen et al. 1995) as HS0129+2933. It has subsequently been suggested to be a member of the SW Sex subclass of novalike variables by Rodríguez-Gil (2005), who measured an orbital period of 3.35 hr for the system.

The study of eclipsing cataclysmic variables is valuable because it provides the opportunity to study the radiative properties of accretion disks through analysis of the eclipse profiles. In an attempt to further elucidate the properties of this long-neglected system, we have obtained extensive, time-resolved, multi-color CCD photometry of the eclipses of TT Tri, and subsequently analyzed the resulting eclipse profiles with a parameter-fitting eclipse model. In this paper we present the results of that study.

¹Current Address: Department of Astronomy, University of Minnesota, 116 Church Street S. E., Minneapolis, MN 55455

2. Observations

Observations of TT Tri² were carried out during 14 nights in 2005 September – December using the Mount Laguna Observatory 1 m reflector. On each night a series of exposures (typically 30 s) were taken through either a Johnson-Cousins B , V , R , or I filter (see Bessel 1990), and imaged on a Loral 2048² CCD. To increase the time-sampling efficiency, only a 400×400 subsection of the full array was read out. The subsection was centered on TT Tri and included several nearby stars that were used as comparison objects for differential photometry. A summary of observations is presented in Table 1.

The data were processed in a standard fashion (bias subtraction and flat-fielding) using IRAF.³ The individual images were subsequently aligned to a common coordinate system and magnitudes for TT Tri and the two comparison stars were then determined using the *IRAF* APPHOT package. Atmospheric extinction variations were removed to first order by dividing the flux of TT Tri by a nearby comparison star. The B and V differential light curves were then placed on an absolute scale by calibration of the comparison star against the standard stars in Landolt (1992). During the 14 nights of observation, we observed a total of 22 eclipses – six in B and R , seven in V , and three in I . The resulting eclipse light curves are displayed in Figures 1 and 2, with the mean photometric parameters given in Table 2. The uncertainties in the mean magnitudes for the B and V light curves reflect systematic variations in the disk luminosity (including short-term “flickering”) that presumably results from fluctuations in the mass transfer rate. The individual photometric measurements have uncertainties of ~ 0.03 mag.

3. TT Tri Ephemeris

Despite its identification as an eclipsing binary nearly 30 years ago, there are no published eclipse timings available for TT Tri, so we have used our 22 eclipse timings of TT Tri to establish one. Following earlier studies, the times of mid-eclipse have been determined by fitting a parabola (a second order polynomial with no cross term) to the lower half of the eclipse profile and taking the minimum to be the time of mid-eclipse. A linear least-squares fit of the resulting mid-eclipse times (see Table 3) yields the following ephemeris for TT Tri:

² $\alpha = 01 : 31 : 59.86$, $\delta = +29 : 49 : 22.1$ (epoch 2000.0); $\ell = 133^\circ$, $b = -32^\circ$ (Downes et al. 2001).

³IRAF (Image Reduction and Analysis Facility) is distributed by the National Optical Astronomy Observatories, which are operated by AURA, Inc., under cooperative agreement with the National Science Foundation.

$$T_{\text{mid-eclipse}} = \text{JD}_{\odot} 2,453,618.953(3) + 0.1396369(4) E. \quad (1)$$

Residuals of the individual eclipse timings with respect to this ephemeris are also given in Table 3, and are plotted as a function of cycle number in Figure 3. The relatively short (~ 3 month) interval spanned by our observations does not allow us to assess the long-term stability of the orbital period of TT Tri.

4. The Eclipse Model

The TT Tri data have been analyzed using the latest version of parameter-fitting eclipse modeling program described in Shafter & Misselt (2006, hereafter SM06). The model considers four principal sources of light from the system: the white dwarf, the secondary star, the accretion disk (including a rim), and the bright spot where the inter-star mass transfer stream impacts the periphery of the disk. The model light curve flux at a given orbital phase is computed by summing the contribution from the secondary star and the unocculted regions of the remaining three sources of radiation. The fluxes from all four sources of radiation have been corrected via the use of a linear limb-darkening law with passband-specific coefficients given in van Hamme (1993). Although the model fits only the shapes and depths of the eclipse profiles, we compute a model $B - V$ color from the assumed blackbody fluxes using the transformations given in Matthews & Sandage (1963) that can be compared with the observed $B - V$ color.

As in previous studies, the disk in TT Tri is assumed to radiate like an optically-thick blackbody, characterized by a radial, power-law temperature profile. A comprehensive mathematical description of the model computations can be found in SM06. As a point of clarification, we note that the expressions for the disk (surface and rim) and the primary and secondary star fluxes (eqns. 3–8) of SM06 imply that the specific intensity of the radiating surfaces can be approximated by the Planck function multiplied by the linear limb darkening law. However, the Planck function does not represent the specific intensity normal to the radiating surface, as assumed, but rather the specific intensity integrated over all emergent angles. The use of model atmospheres in lieu of blackbody radiation in future versions of the code would solve this problem, but in the meantime the fluxes given in SM06 can be approximately corrected by dividing the relevant expressions by the factor $1 - \mu_{\lambda}/3$ that results when the linear limb darkening expression is integrated over 2π steradians. Fortunately, the omission of this factor did not affect our earlier results significantly since the eclipse model uses relative fluxes to compute normalized light curve intensities; thus, the factors of $1 - \mu_{\lambda}/3$ (which are similar for all sources of light in the system) effectively cancel

in the computation of the model light curves.

In the case of a steady-state accretion disk, the relation between the effective temperature and radius is given by (e.g. Pringle 1981):

$$\sigma T_{\text{eff}}^4(r) = \frac{3GM_1\dot{M}}{8\pi r^3} \left[1 - \sqrt{\frac{R_{\text{in}}}{r}} \right], \quad (2)$$

where R_{in} is the inner radius of the disk. For $r \gg R_{\text{in}}$, eqn. (2) reduces to the well-known relation $T_{\text{eff}}(r) \propto r^{-3/4}$. However, the temperature we consider in our model is actually a brightness temperature, not an effective temperature. Thus, to generalize the temperature dependence with radius, we allow for temperature gradients that deviate from the steady state value. In previous papers, we have assumed $T_{\text{br}}(r) \propto r^{-\alpha}$, however, this simple parameterization will overestimate the disk temperature at small radii. Thus, in our present study, we employ a modified power law given by:

$$T_{\text{br}}(r) = T_{\text{d}} \left(\frac{R_{\text{d}}}{r} \right)^{\alpha} \left[1 - \sqrt{\frac{R_{\text{in}}}{r}} \right]^{(\alpha/3)}, \quad (3)$$

where T_{d} is the brightness temperature of the rim at the outer edge of the disk. Since the disk's brightness temperature profile (as fit by our model) is not precisely the same as its effective temperature profile, a steady state disk will not necessarily be characterized by $\alpha = 0.75$.

One of the significant advantages of the inclusion of a disk rim is that the bright spot can be more easily modeled. The presence of the disk rim provides both an isotropic and an anisotropic component to the bright spot radiation. The isotropic component of the bright spot is produced as in Shafter et al. (2000). by radiation from a region of the disk's surface defined by the intersection of a circular area of radius $0.2 R_{\text{d}}$ (centered on the point of intersection of the mass-transfer stream and the disk perimeter) and the accretion disk. The anisotropic component is produced by radiation from the corresponding azimuthal region of the disk rim. As in earlier studies, the bright spot is assumed to radiate like a blackbody, with the bright spot temperature parameterized by a multiplicative factor, χ_{s} , applied to the local disk temperature in the bright spot region.

The white dwarf primary star and the secondary star are assumed to radiate as blackbodies of temperature T_1 and T_2 , respectively, with the tidally-distorted shape of the Roche-lobe-filling secondary star fully taken into account. The effects of gravity darkening and irradiation of the secondary star by the primary component are neglected in our model since their effects are expected to be minimal in our analysis. Not only does the secondary star contribute a small fraction of the system's total light, we only model a limited range of

orbital phase near primary eclipse. The radii of the white dwarf and secondary stars are computed from the orbital period and mass ratio as described in Shafter et al. (2000).

4.1. Input Parameters

The input parameters required by the model are summarized in Table 4. They can be divided into two general categories: fixed parameters and fitting parameters. The fixed parameters are those parameters that are either known, a priori, such as the orbital period, or those whose values can be estimated using assumptions implicit in the model. The fitting parameters, on the other hand, cannot be specified initially, and are varied during the fitting procedure.

Since the orbital period ($P=3.35$ hr) and eclipse width ($\Delta\phi = 0.035$) are known, the masses and dimensions of the binary system can be computed once the mass ratio, $q(= M_2/M_1)$ is specified (e.g. see Shafter et al. 2000). Unfortunately, the mass ratio of TT Tri is unknown. For a given secondary star mass, possible values of the mass ratio can be constrained both by the requirement that the white dwarf star not exceed the Chandrasekhar limit, and by the requirement for stable mass transfer. The dependence of M_2 on q is weak, and to first order the mass of the secondary star can be expressed as a function of the orbital period alone. From Warner (1995, eqn. 2.100) we have $M_2/M_\odot \simeq 0.065P^{5/4}(\text{hr})$; for an orbital period of 3.35 hr, we therefore estimate $M_2 \simeq 0.3M_\odot$. Thus, the requirement that $M_1 < M_{\text{ch}}$ leads to a lower limit of $q \gtrsim 0.25$. A firm upper limit on the mass ratio is more difficult to establish. Models that treat the secondary star as a fully convective polytrope require $q \lesssim 2/3$ for stable mass transfer (e.g. Politano 1988). However, more recent studies suggest that stable accretion may be possible at mass ratios approaching unity (e.g. see Han et al. 2002, and references therein). Thus, the mass ratio of TT Tri must lie in the range $0.25 \lesssim q \lesssim 1.0$. Given that $M_2 \sim 0.3M_\odot$ and the average white dwarf masses in novalike systems is believed to be of order $0.8 M_\odot$ (Smith & Dhillon 1998), it would appear likely that the actual mass ratio of TT Tri lies closer to the lower end of this range. Nevertheless, in order to explore the effect of the mass ratio on our analysis, we have explored solutions for three representative mass ratios: $q = 0.3$, $q = 0.6$, and $q = 0.9$. Following the analysis described in Shafter et al. (2000), the possible masses, dimensions, and orbital inclinations of the TT Tri system have been computed for our representative mass ratios, and are summarized in Table 5.

In addition to the mass ratio, the spectral type and temperature of the secondary star can be estimated prior to beginning the fitting procedure. In their statistical study of the properties of cataclysmic variable stars, Smith & Dhillon (1998) found an empirical relation

between the orbital period and spectral type of the secondary star. For an orbital period of 3.35 hr, the most likely spectral type is \sim M4V. According to Popper (1980) a star with this spectral type is expected to have a temperature of \sim 3400 K. Thus, we have chosen to fix $T_2 = 3400$ K, and not vary this parameter during the fitting procedure. If the secondary star in TT Tri deviates significantly from the mean properties of CVs with similar orbital periods and measured spectral types (e.g. because it deviates from the main-sequence mass-radius relation), our estimate of T_2 , and thus the light contributed by the secondary star, would clearly become less reliable.

Another input parameter that can be constrained to a limited extent is the disk rim thickness, $h_r = h/R_d$, where h is the height of the rim perpendicular to the plane of the disk and R_d is the disk radius. As discussed in SM06, studies by Meyer & Meyer-Hofmeister (1982) and Smak (1992) have shown that the rim height can be approximated by $h_r \simeq 0.038 \dot{M}_{16}^{3/20}$ (Warner 1995; eqn. 2.52). For plausible mass accretion rates between $\sim 10^{16}$ g s $^{-1}$ and $\sim 10^{18}$ g s $^{-1}$, we estimate rim heights in the range of $h_r \sim 0.04$ to $h_r \sim 0.08$. To bracket the range, we consider specific rim heights of both $h_r = 0.04$ and $h_r = 0.08$ in our models of TT Tri. We chose not to consider a finer grid of possible rim heights given that the relatively low inclination of the TT Tri system makes it unlikely that the precise choice of rim thickness will have a significant impact on the model results.

The values of the remaining parameters, the “fitting parameters”, which include the radial disk temperature parameter α , and the temperatures of the disk rim, bright spot, and component stars, are constrained through the model fit.

5. Light-Curve Fitting

For ease of computation, the individual light curves for each color were averaged together before beginning the fitting procedure. All but one of the 22 eclipse light curves were considered for the modeling routine. The initial V light curve from 2006 September 05 had a different time resolution from the rest of the data, and was used solely in the determination of the ephemeris. The remaining light curves were converted to orbital phase, and placed on a relative intensity scale. The light curves for each color were then combined by phase-binning the data ($\Delta\phi = 0.005$) in the phase range $-0.2 < \phi < 0.2$, and averaging. The four resulting $BVRI$ light curves were then normalized by their out-of-eclipse light levels. Since the post-eclipse light level is systematically brighter and less stable than the pre-eclipse level in all colors, we arbitrarily assigned the pre-eclipse data a relative weight twice that of the post-eclipse data when computing the normalization.

In previous studies of eclipsing novalike variables, the brightness temperature profiles of the accretion disks are often found to be significantly less steep than one would expect for steady-state accretion (e.g. see Bíró 2000, Robinson et al. 1999, Rutten et al. 1992). Smak (1994) and Knigge et al. (2000) have shown that the addition of a rim can steepen the derived temperature profile of the disk. More recently, in their study of V Per, SM06 found that the inclusion of a disk rim, or a truncation of the inner accretion disk (as might arise from the partial disruption of the disk by the white dwarf’s magnetic field), or both, resulted in best-fitting models with steeper values of the radial disk temperature exponent, α . In the case of TT Tri, the shallower eclipses and lower inclination angle reduces the importance of the disk rim (e.g. Smak 1994). However, a truncated inner disk might still have a significant effect on the value of α . To explore this possibility further, we have computed eclipse models with truncated inner disks. A value of $R_{\text{in}} = 0.2R_{\text{L1}}$, which was adopted by SM06 in their study of V Per, proved to be too large to produce plausible fits to the TT Tri data. Instead, we considered two sets of models with less extensive inner disk disruptions: one set with $R_{\text{in}} = 0.05R_{\text{L1}}$, and the other with $R_{\text{in}} = 0.10R_{\text{L1}}$.

To begin the fitting procedure, we select plausible ranges of values for the five fitting parameters, indicated in Table 4 as “variable”. Each parameter is then varied one at a time through a suitable range while the remaining parameters are held constant. In this way a 5-dimensional parameter space of models is explored for plausible solutions. The goodness of fit at each stage is determined using a standard χ^2 test. The deviations between the model and the data are determined for each of the four colors, and the final χ^2 statistic is determined by weighting each of the colors equally. Since we model the light curve near eclipse only, the calculation of χ^2 has been restricted to orbital phases between $\phi = -0.08$ and $\phi = 0.08$, which corresponds roughly to the time just prior to the onset of disk ingress to the completion of bright-spot egress. The range over which each parameter is varied has been chosen to be sufficiently large so that all plausible model solutions were explored. A thorough sampling required eight values to be considered for each fitting parameter. Thus, a total of 32,768 ($= 8^5$) models were computed for each mass ratio and rim thickness considered. The best-fitting solutions for our grid of models standard disk (SD) and truncated disk (TD) models are given Tables 6 and 7.

5.1. The Model Solution Distributions

As found previously in our studies of other eclipsing CVs, exploring the matrix of possible solutions reveals that many combinations of parameters produce good fits to the data. The goal is to determine which particular combination of parameters best represents

the true model for TT Tri. The best model fits are characterized by a reduced chi-square, $\chi^2_\nu \simeq 1.1$; however, a wide range of parameters give acceptable fits to the light curves.

To explore the range of plausible solutions, frequency distributions for the 100 best-fitting models were constructed for each of the five fitting parameters, and for the the model $B - V$ color. As examples, the distributions for the standard disk models with $h_r = 0.04$ for our three representative mass ratios are shown in Figures 4–6. The mean and standard deviation of each parameter distribution, along with the mean χ^2_ν for all models are summarized in Tables 8 and 9. As long as the number of model solutions included in the distributions is sufficiently small so that $\langle \chi^2_\nu \rangle \lesssim 2.0$ (which represents a plausible fit to the data), the distribution means do not depend strongly on the precise number of model solutions included in the distributions. The $\langle \chi^2_\nu \rangle$ values suggest that the higher mass ratio ($q = 0.6$ and $q = 0.9$) SD and TD models provide better fits to the data than do the $q = 0.3$ models, although the latter models cannot be unequivocally ruled out based on their fits alone.

The frequency distributions reveal how well a given parameter is constrained by the model fit, with the mean and standard deviation providing an estimate of the parameter’s optimum value, and a quantitative assessment of its uncertainty. One of the more tightly constrained parameters is the disk radius, R_d , where a radius of $\sim 40 - 60\%$ of the distance to the inner Lagrangian point is required by virtually all the models. The value of this parameter is primarily determined by the phase width where the disk eclipse begins and ends, and is relatively insensitive to other system parameters (e.g. Sulkanen et al. 1981). The maximum size of the accretion disk is limited to the tidal radius, which for TT Tri is $\sim 0.74R_{L1}$ for $q = 0.3$, $\sim 0.68R_{L1}$ for $q = 0.6$, $\sim 0.62R_{L1}$ for $q = 0.9$ (Warner 1995, eqn. 2.61). Given that the re-distribution of angular momentum in a steady-state disk is expected to result in an increase in the disk radius out to near the tidal radius, it appears once again that the higher mass ratio models, where the disk fills a greater fraction of the tidal radius, are perhaps more realistic.

Despite the fact that the best-fitting SD models are characterized by values of $\alpha \simeq 0.6$, the distributions reveal that viable solutions are possible with the nominal steady-state value of $\alpha \simeq 0.75$. If we force the SD models to have $\alpha = 0.75$, the $q = 0.6$ and $q = 0.9$ models provide significantly better fits to the data than do the $q = 0.3$ models, with little change in the best-fitting values of the other parameters. For this reason, and because the higher mass ratio models produce a better fit to the data and yield a more plausible disk radius, it appears likely once again that the mass ratio of TT Tri lies in the upper end of the allowed range.

Despite the indirect evidence for a mass ratio near the upper end of the allowed range, our eclipse modeling does not enable a precise value of the mass ratio in TT Tri to be

determined, as is evidenced by the fact that both the $q = 0.6$ and $q = 0.9$ models, for example, produce nearly identical fits to the data. Fortunately, as can be seen from Tables 6 and 7, and from Figures 4–6, the properties of the accretion disk determined by our model fit are quite insensitive to the adopted mass ratio. Given that a mass ratio of $q = 0.9$ is near the limit of mass transfer stability, and would be unusual for a CV with such a short orbital period, we consider the $q = 0.6$ models to best represent the TT Tri system. Figure 7 shows the best-fitting $q = 0.6$ SD model plotted together with the phased eclipse data.

As is typical for a novalike variable, the light curves do not exhibit any significant asymmetry of the eclipse profile, and there is no prominent “hump” prior to eclipse, so it is not surprising that none of the models considered required a significant temperature enhancement from the bright spot in the system. Furthermore, the eclipse profile, which lacks the sharp transitions on ingress and egress characteristic of the white dwarf eclipse suggest that the white dwarf star does not contribute significantly to the system light (except in the case of the TD models where the white dwarf luminosity partially compensates for the inner disk radiation). Thus, as expected, none of the best-fitting SD models required a particularly luminous (hot) white dwarf.

6. Discussion

6.1. Disk Structure

The geometry of the TT Tri system can be visualized by referring to Figure 8, which shows a pictorial representation of the system geometry at mid-eclipse for our $q = 0.6$ model. As suggested by the relatively shallow eclipse depths ($\sim 50\%$ of the out-of-eclipse level), the white dwarf is just barely eclipsed at $\phi = 0$. Not only does the relatively low orbital inclination for TT Tri result in only partial eclipse of the accretion disk, it also minimizes the contribution of the disk rim to the overall disk light. Thus, unlike our models for the high-inclination system, V Per (SM06), the thickness of the disk rim did not have a significant effect on our model solutions.

Although the TD models are generally characterized by higher values of the disk temperature parameter, α , viable SD models can be found with steep temperature profiles ($\alpha \simeq 0.75$) typical of what is expected for a steady-state disk. Thus, there is no compelling evidence for a truncated inner disk in TT Tri based on our eclipse studies. Nevertheless, the system has not yet been extensively studied, and perhaps future observations (e.g. polarimetry) may reveal signatures of a magnetic white dwarf in this system.

6.2. Correlations Between Model Parameters

Insights into the effect that the various input parameters have on acceptable model solutions can be found by exploring correlations between the parameters. We begin by considering our expanded set of model solutions defined by $\chi^2_\nu < 2.0$, which allows potential correlations to be studied over an expanded range in parameter space. Correlations between pairs of parameters are explored by allowing them to vary while holding the remaining parameters fixed at their optimum values. For a total of five fitting parameters, there are a total of 10 such pairings. As a representative example, Figure 9 shows the correlations based on our best-fitting $q = 0.6$ SD model.

For the standard disk models, the most highly correlated parameter pairs involve R_d , T_d , and α , which together determine the disk luminosity. In cases where the accretion disk is completely occulted at mid-eclipse (e.g. high inclination systems and/or longer orbital period systems with higher mass ratios), the relative eclipse depth is determined uniquely by the integrated disk luminosity. For a constant disk luminosity, the radial temperature parameter α should be negatively correlated with the temperature at the disk periphery, T_d , and the disk radius, R_d , as was indeed observed in our earlier studies of GY Cnc (Shafter et al. 2000) and EX Dra (Shafter & Holland 2003). However, as shown in our recent study of V Per, another system where the disk is never completely obscured, the eclipse depth no longer uniquely defines the disk luminosity. The normalized eclipse depth can be achieved with a relatively low-luminosity disk with a shallow radial temperature gradient (small α), and a cooler outer disk temperature, or a smaller outer disk radius, or both. Alternatively, the required eclipse depth can be achieved with a more luminous disk characterized by a steeper temperature profile coupled with a higher outer disk temperature, a larger outer disk radius, a bright disk rim, or some combination of the three. As the radiation from the outer disk is increased, the inner disk luminosity must increase to compensate, requiring a steeper temperature gradient and a higher value of α . Thus, for a given disk radius and rim thickness, α should be *positively* correlated with the outer disk (rim) temperature, T_d , as was observed in the case of V Per, and now for TT Tri as shown in Figure 9.

6.3. Potential Model Constraints from the Disk Luminosity

Although a range of models can produce acceptable fits to the data, as just discussed they need not represent the same disk luminosities. Thus, it is worth exploring whether the disk luminosity expected for the TT Tri system can be used to constrain the set of viable models. The disk luminosities can be explored through two independent approaches: directly from our model fluxes, and from an estimate of the mass accretion rate inferred from our

models.

In the first approach, we can compare the ratio of our model V fluxes for the disk and secondary star as viewed from an inclination angle of $i = 0$ (i.e. “face-on”). This quantity, $\eta_{d,s} = F_V^d(i = 0)/F_V^s(i = 0)$, is given in Tables 10 and 11 for our best-fitting SD and TD models, respectively. If we ignore limb-darkening and assume a spherical secondary star and a flat circular disk, then the luminosity ratio is approximately equal to half the model flux ratio (a flat disk has half the surface area of a sphere). Thus, $L_V^d/L_V^s \simeq \eta_{d,s}/2$, and an estimate of the secondary star’s luminosity will yield a crude estimate for the disk luminosity (neglecting the small contribution of the rim to the overall light.). As an example, the flux ratio of our best-fitting $q = 0.6$ SD model is $\eta_{d,s} = 126$, which represents a luminosity ratio of ~ 63 . Thus, we estimate the disk in this model to be ~ 4.5 mag brighter than the secondary star. An estimate of $M_{V,2}$ can be found given the secondary star’s spectral type, which we estimated earlier to be $\sim M4V$. For a main-sequence secondary star of radius $R_2 = 0.34 R_\odot$ (Table 5) and spectral type M4V, we find $M_{V,2} \simeq 11.5$ (Popper 1980). Thus, for this model, we estimate an absolute visual magnitude for the accretion disk, and in effect for the TT Tri system (the white dwarf and secondary star contribute little V light compared to the disk), to be $M_V \sim 7.0$. This value is roughly 1 – 1.5 magnitudes fainter than expected for a $P = 3.35$ hr novalike system (e.g. Warner 1987). If we consider the truncated inner disk model ($R_{in} = 0.10 R_{L1}$) with $\eta_{d,s} = 131$, we find a similar value with $M_V \sim 6.9$.

As a check on these results, following SM06 we can also make a rough estimate of the disk luminosity from an estimate of the mass transfer rate coupled with the \dot{M} vs. M_V relation from Tylanda (1981). By assuming the disk is in a steady-state, and adopting the model radius and temperature of the outer disk (rim), we can estimate the mass accretion rate for a given model from eqn (2). Specifically,

$$\dot{M} = \frac{8\pi R_d^3 \sigma T_d^4}{3GM_1} \left[1 - \sqrt{\frac{R_{in}}{r}} \right]^{-1} \text{ g s}^{-1}. \quad (4)$$

Mass transfer rates ($\dot{M}_{17} = \dot{M}/10^{17} \text{ g s}^{-1}$) for our best-fitting models are given in Tables 10 and 11. These values should be considered rough estimates given that we are implicitly taking $T_{eff} = T_{br}$, and neglect any heating of the outer disk that may be caused by irradiation from the white dwarf and inner disk. For the specific case of the $q = 0.6$ SD model we have converted the mass-transfer rate to an equivalent M_V through the relation given in Table 1 of Tylanda (1981).⁴ We find a value of $M_V \sim 5.8$, which is somewhat brighter, and more

⁴A small correction (~ 0.8 mag) has been applied to the resulting absolute magnitude to account for the difference in M_1 and R_d between Tylanda’s model ($M_1 = 1M_\odot$, $R_d = 5 \times 10^{10} \text{ cm}$) and our model. Following Warner (1995), the correction for R_d has been estimated from the models of Wade (1984).

typical of that expected for a novalike variable, than the value of $M_V \sim 7.0$ estimated earlier from the disk-to-secondary star luminosity ratio.

Since TT Tri does not exhibit dwarf nova eruptions, a further constraint on possible models for this system is provided by the requirement that the mass transfer rate exceed the critical value for stable accretion, \dot{M}_{crit} . A convenient expression for the critical mass transfer rate is given by $\dot{M}_{\text{crit}} \simeq 10^{16} R_{10}^{21/8} M_1^{-7/8} \text{ gm s}^{-1}$, where R_{10} is the radius of the disk in units of 10^{10} cm (e.g. see Shafter et al. [1986], and references therein). Values of \dot{M}_{crit} for our best-fitting models are given in Tables 10 and 11. Most models have mass accretion rates that are slightly above the critical value, which is consistent with the lack of reported dwarf nova eruptions in TT Tri. However, the proximity of the inferred mass transfer rates to the critical value suggests that it would not be surprising if future observations revealed TT Tri to exhibit standstills characteristic of the Z Cam stars.

In summary, the disk luminosities and mass accretion rates for both the SD and TD models are consistent with what is expected for a $P = 3.35$ hr novalike variable. Thus, we are unable to distinguish between the SD and TD classes of models for TT Tri based on these criteria.

6.4. The Distance to TT Tri

The distance to TT Tri can be estimated by comparing the observed brightness at mid-eclipse with estimates of the absolute magnitude of the secondary star ($M_{V,2}$), and the fraction of light it contributes at mid-eclipse. The fraction of light contributed by the secondary star at mid-eclipse, $f_2 = f_V^s(\phi = 0)/f_V^{\text{tot}}(\phi = 0)$, depends on the model considered, and values of f_2 for each model are given in Tables 10 and 11. Generally, the secondary star contributes between 3% and 5% of the light at mid-eclipse. Given that $m_V = 16.42 \pm 0.25$ (see Table 2) at mid-eclipse, we estimate the distance moduli $(m - M)_V$ given in Tables 10 and 11. Within the errors of our measurements, the observed and model $B - V$ colors agree well. Thus, $E(B - V) \simeq 0$, and there is no evidence for any significant reddening along the line of sight to TT Tri.

As a consistency check, the distance to TT Tri can also be determined from a comparison of the out-of-eclipse magnitude with an estimate of the system’s absolute magnitude corrected for inclination. Warner (1987, 1995) gives a correction factor for the conversion of absolute magnitude to *apparent* absolute magnitude of $\Delta M_V(i) = -2.5 \log [(1 + 1.5 \cos i) \cos i]$. For our representative $q = 0.6$ model, $i = 72.6^\circ$, which leads to a correction of ~ 0.9 mag (where we have ignored the small contribution of the disk rim). If we assume that TT Tri has

an absolute magnitude $M_V \simeq 6.4 \pm 0.5$ (the mean of our two estimates from the previous section), and adopt $m_V = 15.61 \pm 0.14$ for TT Tri out of eclipse (see Table 3), we find $(m - M)_V = 8.3 \pm 0.5$, and a corresponding distance of ~ 450 pc. Despite the uncertainties, this value is consistent with our distance estimates based on the observed light from the secondary star at mid-eclipse, giving us confidence in our derived distance to TT Tri. The principal source of uncertainty in our distance estimates arises from the adopted absolute magnitude of the secondary star, which assumes that its properties follow the mean relations for secondary stars in CVs determined by Smith & Dhillon (1998).

7. Conclusions

We have performed the first multicolor eclipse study of the novalike variable TT Tri. The best-fitting model parameters are typical of what is expected for a P=3.35 hr novalike variable, and are relatively insensitive to the adopted mass ratio and rim thickness. Our major conclusions are summarized below:

1) The mass ratio of TT Tri is poorly constrained. As a result, we have considered a wide range of possible values in our analysis: $q = 0.3$, $q = 0.6$, and $q = 0.9$. We found that not only do the higher mass ratio models provide a better fit to the data, they are characterized by disks that are more typical of a system with steady-state accretion (e.g. radii close to their tidal limit with steep radial temperature profiles). Nevertheless, acceptable model fits can be found for $q = 0.3$, and thus lower mass ratios cannot be ruled out by the data. Fortunately, the values for the other fitting parameters are very insensitive to the adopted mass ratio.

2) The radius of the accretion disk in TT Tri extends to $\sim 50\text{--}60\%$ of the distance to the inner Lagrangian point, which is somewhat smaller than the maximum size allowed by tidal effects. The disks in the higher mass ratio models fill a larger fraction of their tidal radius, as expected if the disk is in a state of steady accretion. In the $q = 0.3$ models, the disk extends to only $\sim 70\%$ of the tidal radius, while for the $q = 0.6$ and $q = 0.9$ models the disk extends to $\sim 80\%$ and $\sim 90\%$ of the tidal radius, respectively. This result provides indirect evidence that the mass ratio in TT Tri may be closer to the maximum value allowed for stable accretion, and that the white dwarf may have a relatively low mass ($M_1 \simeq 0.3 - 0.5 M_\odot$).

3) As found in many other novalike systems, the best fitting models of TT Tri are not necessarily characterized by disks with steep radial temperature profiles ($\alpha \simeq 0.75$). For example, SD models with values of α as low as 0.4 were found to provide acceptable fits to the data, particularly in the cases where $q = 0.3$. It is worth recalling that steady-state

accretion does not necessarily require $\alpha = 0.75$. To begin with our models fit brightness temperature, not the effective temperature used in eqn (2). Furthermore, the effects of irradiation of the outer disk from hotter regions near the white dwarf, and the potential cooling effects of winds from the inner accretion disk, both of which would have the effect of reducing the radial disk temperature gradient, have not been included in our models. Despite these caveats, it remains true that the smaller the value of α , the less confident we can be that the disk is in a state of steady accretion.

4) Unlike the case of V Per, where a thick disk rim was required to achieve temperature profiles approaching $\alpha = 0.75$, the thickness of the rim had little effect in TT Tri. However, significantly steeper values of α were found when the inner disk was truncated, as one would expect if the white dwarf is magnetic. A likely explanation for the different behavior between V Per and TT Tri is that the orbital inclination is significantly lower in TT Tri. A lower inclination will make the disk rim less important (e.g. Smak 1994), while making the contribution of the inner disk relatively more important. Despite the fact that the TD models are characterized by significantly larger values of α , as just discussed, steady-state solutions were found for the SD models as well. Thus, in our modeling, we find no compelling evidence for a truncated inner disk in TT Tri.

5) We estimate that TT Tri is characterized by a mass accretion rate, $\dot{M} \sim 2 \times 10^{17} \text{ g s}^{-1}$, which is just above the critical rate for stable accretion. Given the proximity of the accretion rate to the critical value, it is possible that future observations of TT Tri may reveal dwarf nova eruptions similar to those seen in the Z Cam stars, where the system fluctuates between state of stable and unstable accretion (e.g. Shafter et al. 2005). The TD models are characterized by somewhat higher accretion rates, making them more typical of novalike systems with stable accretion.

6) Finally, by comparing the observed brightness of TT Tri, both in and out of eclipse, with properties of the secondary star and accretion disk, we find that the system likely lies at a distance of $\sim 400 - 500 \text{ pc}$ from Earth. The principle source of error in this estimate comes from uncertainty in the assumed properties of the secondary star.

We thank Jerry Orosz for computing pictorial representations of the system geometry near mid-eclipse, and an anonymous referee for numerous suggestions that helped to improve our presentation. Our eclipse model is based in part on occultation kernel subroutines kindly provided by K. Horne. This research was partially supported by a grant from NASA administered by the American Astronomical Society.

REFERENCES

- Bíró, I. B. 2000, A&Ap, 364, 573.
- Bessel, M. S. 1990, PASP, 102, 1181.
- Downes, R. A., Webbink, R. F., Shara, M. M., Ritter, H., Kolb, U., & Duerbeck, H. W. 2001, PASP, 113, 764.
- Hagen, H.-J., Groote, D., Engels, D., & Reimers, D. 1995, A&AS, 111, 195.
- Han, Z., Podsiadlowski, Ph., Maxted, P. L. F., Marsh, T. R., & Ivanova, N. 2002, MNRAS, 336, 449.
- Knigge, C., Long, K. S., Howard, D. W., Szkody, P., & Dhillon, V.S. 2000, ApJ, 539, L49.
- Landolt, A. U. 1992, AJ, 104, 340.
- Matthews, T. A. & Sandage, A. R. 1963, Ap. J., 138, 30.
- Meyer, F., & Meyer-Hofmeister, E. 1982, A&A, 106, 34.
- Pringle, J. E. 1981, Ann. Rev. Astr. Ap., 19, 137.
- Politano, M. 1988, Ph.D. Thesis, University of Illinois.
- Popper D. M. 1980, Ann. Rev. Astr. Ap., 18, 115.
- Robinson, E. L., Wood, J. H., & Wade, R. A. 1999, ApJ, 514, 952.
- Rodríguez-Gil, P. 2005, *The Astrophysics of Cataclysmic Variables and Related Objects*, ASP Conference Series, 330, 335.
- Romano, G. 1978a, IBVS, 1421.
- Romano, G. 1978b, IBVS, 1433.
- Rutten, R. G. M., van Paradijs, J., Tinbergen, J. 1992, A&Ap, 260, 213.
- Shafter, A. W., Cannizzo, J. K., & Waagen, E. O. 2005, PASP, 117, 931
- Shafter, A. W., Clark, L. L., Holland, J. N., & Williams, S. J. 2000, PASP, 112, 1467
- Shafter, A. W. & Holland, J. N. 2003, PASP, 115, 1105
- Shafter, A. W. & Misselt, K. A. 2006, ApJ, 644, 1104 (SM06)
- Shafter, A. W., Wheeler, J. C., & Cannizzo, J. K. 1986, ApJ 305, 261.
- Sharov, A. S., Goranskij, V. P., & Samus, N. N. 1992, IBVS, 3756.
- Smak, J. 1992, AcA, 42, 323.
- Smak, J. 1994, AcA, 44, 265.
- Smith, D. A., & Dhillon, V. S. 1998, MNRAS, 301, 767.

- Sulkanen, M. E., Brasure, L. W., & Patterson, J. 1981, ApJ, 244, 579.
- Tylenda, R. 1981, AcA, 31, 127.
- Wade, R. A. 1984, MNRAS, 208, 381.
- Warner, B. 1995, Cataclysmic Variable Stars, Cambridge Univ. Press.
- Warner, B. 1987, MNRAS, 227, 23.
- van Hamme, W. 1993, AJ, 106, 2096

Table 1. Summary of Observations

UT Date	UT Time (start of observations)	Time Resolution ^a (sec)	Number of Exposures	Filter
2005 Sep 05	08:19:00.70	22.06	487	<i>V</i>
2005 Oct 26	05:42:32.10	32.07	222	<i>B</i>
2005 Oct 27	04:26:01.70	32.07	320	<i>I</i>
2005 Nov 04	03:48:41.00	32.05	354	<i>B</i>
2005 Nov 04	07:07:03.40	32.05	190	<i>B</i>
2005 Nov 05	02:33:00.30	32.06	750	<i>R</i>
2005 Nov 06	04:00:00.00	32.06	563	<i>I</i>
2005 Nov 22	01:29:00.70	32.06	177	<i>R</i>
2005 Nov 22	05:13:01.00	32.05	90	<i>V</i>
2005 Nov 28	01:38:01.00	32.06	151	<i>B</i>
2005 Nov 28	05:00:00.00	32.15	121	<i>B</i>
2005 Nov 29	03:55:30.80	32.06	278	<i>I</i>
2005 Nov 29	06:34:00.40	32.05	300	<i>R</i>
2005 Nov 30	03:40:30.50	32.07	500	<i>V</i>
2005 Nov 30	08:08:23.30	32.05	66	<i>V</i>
2005 Dec 01	01:58:31.00	32.06	350	<i>V</i>
2005 Dec 01	05:17:00.40	32.06	360	<i>V</i>
2005 Dec 21	02:27:00.00	32.06	170	<i>B</i>
2005 Dec 22	02:12:00.90	32.06	171	<i>V</i>
2005 Dec 22	05:06:00.80	32.06	204	<i>R</i>
2005 Dec 24	02:05:00.50	32.06	505	<i>R</i>

^aMean time interval between exposures (integration time plus readout time)

Table 2. Mean Magnitudes and Colors

Photometric Parameter	Effective Wavelength (Å)	Out of Eclipse ^a	Primary Minimum
<i>B</i>	4386	15.69 ± 0.15	16.59 ± 0.30
<i>V</i>	5508	15.61 ± 0.14	16.42 ± 0.25
<i>R</i> ^b	6518	—	—
<i>I</i> ^b	8239	—	—
<i>B</i> – <i>V</i>	0.08 ± 0.20	0.17 ± 0.39

^aThe mean out-of-eclipse magnitude was computed with the pre-eclipse level weighted twice that of the post-eclipse level, as described in the text.

^bThe *R* and *I* photometry was not calibrated.

Table 3. Eclipse Timings

HJD (mid-eclipse) (2,400,000+)	Cycle Number (E)	Filter	$O - C$ ($\times 10^3$ day)
53618.9531...	0.	V	0.501730
53669.7801...	364.	B	−0.315169
53670.7576...	371.	I	−0.222475
53678.7171...	428.	B	−0.083822
53678.8564...	429.	B	−0.344723
53679.6950...	435.	R	0.405872
53679.8339...	436.	R	−0.361029
53680.8110...	443.	I	−0.755334
53696.5913...	556.	R	0.632873
53696.7305...	557.	V	0.213972
53702.5952...	599.	B	0.120137
53702.7347...	600.	B	−0.058764
53703.7122...	607.	I	0.028931
53703.8519...	608.	R	0.126030
53704.6893...	614.	V	−0.314375
53704.8296...	615.	V	0.352724
53705.6671...	621.	V	0.012319
53705.8067...	622.	V	−0.043582
53725.6346...	764.	B	−0.555499
53726.6128...	771.	V	0.206196
53726.7523...	772.	R	0.093295
53728.7075...	786.	R	0.360683

Table 4. Model Input Parameters

Parameter	Definition	Value ^a
P	Orbital Period, P	3.35 hr
q	Mass ratio, M_2/M_1	0.3, 0.6, 0.9
$\Delta\phi$	Eclipse phase width	0.035
i	Orbital inclination	computed
α	Disk temperature parameter	variable (0.25–0.95)
R_d	Disk radius	variable (0.35–0.70)
R_{in}	Inner disk radius	R_1 , $0.05R_{L1}$, $0.10R_{L1}$
h_r	Disk rim parameter	0.04, 0.08
T_d	Temperature of disk perimeter	variable (5000–12000K)
R_1	Radius of white dwarf	computed
R_2	Radius of secondary star	computed
T_1	Temperature of white dwarf	variable (10000–80000K)
T_2	Temperature of secondary star	3400 K
χ_s	Bright spot temperature factor	variable (1.0–2.4)
R_s	Bright spot radius	$0.2R_d$

^aWhere given explicitly, the values are fixed and not varied during the fitting procedure. The values of “variable” parameters are determined by the model during the fitting procedure, while the “computed” values are calculated by the model for a given mass ratio.

Table 5. Binary Parameters

Parameter	$q = 0.3$	$q = 0.6$	$q = 0.9$
$i(^{\circ})$	76.1	72.6	70.4
$a(R_{\odot})$	1.17	1.01	0.95
$R_{L1}(a)$	0.62	0.55	0.51
$R_1(10^{-2} R_{\odot})$...	0.94	1.48	1.75
$M_1(M_{\odot})$	0.86	0.45	0.31
$R_2(R_{\odot})$	0.33	0.34	0.35
$M_2(M_{\odot})$	0.26	0.27	0.28

Table 6. Standard Disk Model Grid Solutions

Parameter	$q = 0.3$		$q = 0.6$		$q = 0.9$	
	$h_r = 0.04$	$h_r = 0.08$	$h_r = 0.04$	$h_r = 0.08$	$h_r = 0.04$	$h_r = 0.08$
$R_d(a)$	0.31	0.31	0.30	0.30	0.28	0.28
$R_d(a)_{\text{lim}}^{\text{a}}$	0.46	0.46	0.38	0.38	0.32	0.32
$R_d(R_{\text{L1}})$	0.50	0.50	0.55	0.55	0.55	0.55
α	0.45	0.55	0.55	0.55	0.65	0.65
$T_1(10^3 \text{ K})$	10.0	20.0	10.0	20.0	10.0	10.0
$T_d(10^3 \text{ K})$	7.0	8.0	7.0	7.0	7.0	7.0
χ_s	1.2	1.2	1.6	1.4	1.6	1.4
$(B - V)_o$	0.21	0.10	0.14	0.15	0.09	0.11
$\chi_{\nu, \text{min}}^2$	1.67	1.86	1.15	1.36	1.15	1.30

^aThe limiting tidal radius of the disk computed using eqn (2.61) of Warner (1995).

Table 7. Truncated Disk Model Grid Solutions

Parameter	$q = 0.3$		$q = 0.6$		$q = 0.9$	
	$R_{\text{in}} = 0.05R_{\text{L1}}$	$R_{\text{in}} = 0.10R_{\text{L1}}$	$R_{\text{in}} = 0.05R_{\text{L1}}$	$R_{\text{in}} = 0.10R_{\text{L1}}$	$R_{\text{in}} = 0.05R_{\text{L1}}$	$R_{\text{in}} = 0.10R_{\text{L1}}$
$R_{\text{d}}(a)$	0.31	0.31	0.30	0.30	0.28	0.28
$R_{\text{d}}(a)_{\text{lim}}^{\text{a}}$	0.46	0.46	0.38	0.38	0.32	0.32
$R_{\text{d}}(R_{\text{L1}})$	0.55	0.50	0.55	0.55	0.55	0.55
α	0.75	0.85	0.65	0.85	0.75	0.85
$T_1(10^3 \text{ K})$	40.0	80.0	20.0	30.0	10.0	20.0
$T_{\text{d}}(10^3 \text{ K})$	8.0	8.0	7.0	7.0	7.0	7.0
χ_{s}	1.4	1.2	1.6	1.6	1.6	1.6
$(B - V)_{\circ}$	0.02	0.04	0.11	0.07	0.07	0.09
$\chi^2_{\nu, \text{min}}$	1.49	1.78	1.14	1.48	1.15	1.53

^aThe limiting tidal radius of the disk computed using eqn (2.61) of Warner (1995).

Table 8. SD Model: Distribution Mean Solutions

Parameter	$q = 0.3$		$q = 0.6$		$q = 0.9$	
	$h_r = 0.04$	$h_r = 0.08$	$h_r = 0.04$	$h_r = 0.08$	$h_r = 0.04$	$h_r = 0.08$
$< \chi_\nu^2 >$	1.79	2.01	1.41	1.59	1.47	1.55
$R_d(R_{L1})$	0.52 ± 0.03	0.48 ± 0.03	0.57 ± 0.04	0.54 ± 0.03	0.55 ± 0.05	0.55 ± 0.04
α	0.59 ± 0.10	0.55 ± 0.12	0.66 ± 0.11	0.68 ± 0.12	0.66 ± 0.12	0.71 ± 0.13
$T_1(10^3 \text{ K})$	32.9 ± 13.1	37.7 ± 17.4	16.7 ± 6.26	23.8 ± 10.5	12.9 ± 3.82	17.2 ± 5.73
$T_d(10^3 \text{ K})$	9.08 ± 1.17	9.23 ± 1.49	8.06 ± 1.14	9.05 ± 1.42	7.58 ± 0.97	8.47 ± 1.24
χ_s	1.39 ± 0.14	1.18 ± 0.06	1.62 ± 0.19	1.45 ± 0.14	1.58 ± 0.20	1.47 ± 0.16
$(B - V)_o$	-0.03 ± 0.10	0.00 ± 0.12	-0.01 ± 0.11	-0.05 ± 0.11	0.01 ± 0.11	-0.03 ± 0.11

Table 9. TD Model: Distribution Mean Solutions

Parameter	$q = 0.3$		$q = 0.6$		$q = 0.9$	
	$R_{\text{in}} = 0.05R_{\text{L1}}$	$R_{\text{in}} = 0.10R_{\text{L1}}$	$R_{\text{in}} = 0.05R_{\text{L1}}$	$R_{\text{in}} = 0.10R_{\text{L1}}$	$R_{\text{in}} = 0.05R_{\text{L1}}$	$R_{\text{in}} = 0.10R_{\text{L1}}$
$\langle \chi_\nu^2 \rangle$	1.60	1.98	1.30	1.69	1.40	1.79
$R_{\text{d}}(R_{\text{L1}})$	0.54 ± 0.05	0.49 ± 0.03	0.58 ± 0.04	0.56 ± 0.05	0.57 ± 0.04	0.57 ± 0.05
α	0.76 ± 0.11	0.81 ± 0.11	0.78 ± 0.12	0.87 ± 0.09	0.77 ± 0.12	0.87 ± 0.10
$T_1(10^3 \text{ K})$	42.8 ± 12.4	61.4 ± 10.8	19.5 ± 6.88	40.1 ± 10.8	13.1 ± 4.62	24.1 ± 6.02
$T_{\text{d}}(10^3 \text{ K})$	8.49 ± 0.97	7.72 ± 0.84	7.66 ± 0.99	7.51 ± 1.12	7.28 ± 0.94	6.97 ± 1.07
χ_{s}	1.44 ± 0.18	1.24 ± 0.11	1.67 ± 0.18	1.57 ± 0.18	1.65 ± 0.20	1.57 ± 0.22
$(B - V)_\circ$	-0.05 ± 0.08	0.03 ± 0.07	-0.03 ± 0.09	-0.01 ± 0.08	-0.01 ± 0.09	0.02 ± 0.07

Table 10. SD Models: Derived Properties

Parameter	$q = 0.3$		$q = 0.6$		$q = 0.9$	
	$h_r = 0.04$	$h_r = 0.08$	$h_r = 0.04$	$h_r = 0.08$	$h_r = 0.04$	$h_r = 0.08$
$\eta_{d,s}$	159	274	126	125	103	102
M_V	6.7	6.2	7.0	7.0	7.2	7.2
$\dot{M}_{17} \text{ (g s}^{-1}\text{)}$	1.9	3.3	2.4	2.4	2.4	2.4
$\dot{M}_{\text{crit},17} \text{ (g s}^{-1}\text{)}$	1.3	1.3	1.5	1.5	1.4	1.4
f_2	0.050	0.027	0.053	0.048	0.060	0.055
$(m - M)_V$	8.2	8.9	8.1	8.2	8.0	8.1
$d \text{ (pc)}$	430	590	420	440	390	410

Table 11. TD Models: Derived Properties

Parameter	$q = 0.3$		$q = 0.6$		$q = 0.9$	
	$R_{\text{in}} = 0.05R_{\text{L1}}$	$R_{\text{in}} = 0.10R_{\text{L1}}$	$R_{\text{in}} = 0.05R_{\text{L1}}$	$R_{\text{in}} = 0.10R_{\text{L1}}$	$R_{\text{in}} = 0.05R_{\text{L1}}$	$R_{\text{in}} = 0.10R_{\text{L1}}$
$\eta_{\text{d,s}}$	388	249	133	131	112	93
M_{V}	5.8	6.3	6.9	6.9	7.1	7.3
$\dot{M}_{17} \text{ (g s}^{-1}\text{)}$	5.3	5.0	2.7	3.3	2.5	3.1
$\dot{M}_{\text{crit},17} \text{ (g s}^{-1}\text{)}$	1.7	1.3	1.5	1.5	1.4	1.4
f_2	0.021	0.029	0.050	0.045	0.055	0.058
$(m - M)_{\text{V}}$	9.1	8.8	8.2	8.3	8.1	8.0
$d \text{ (pc)}$	660	570	430	460	410	400

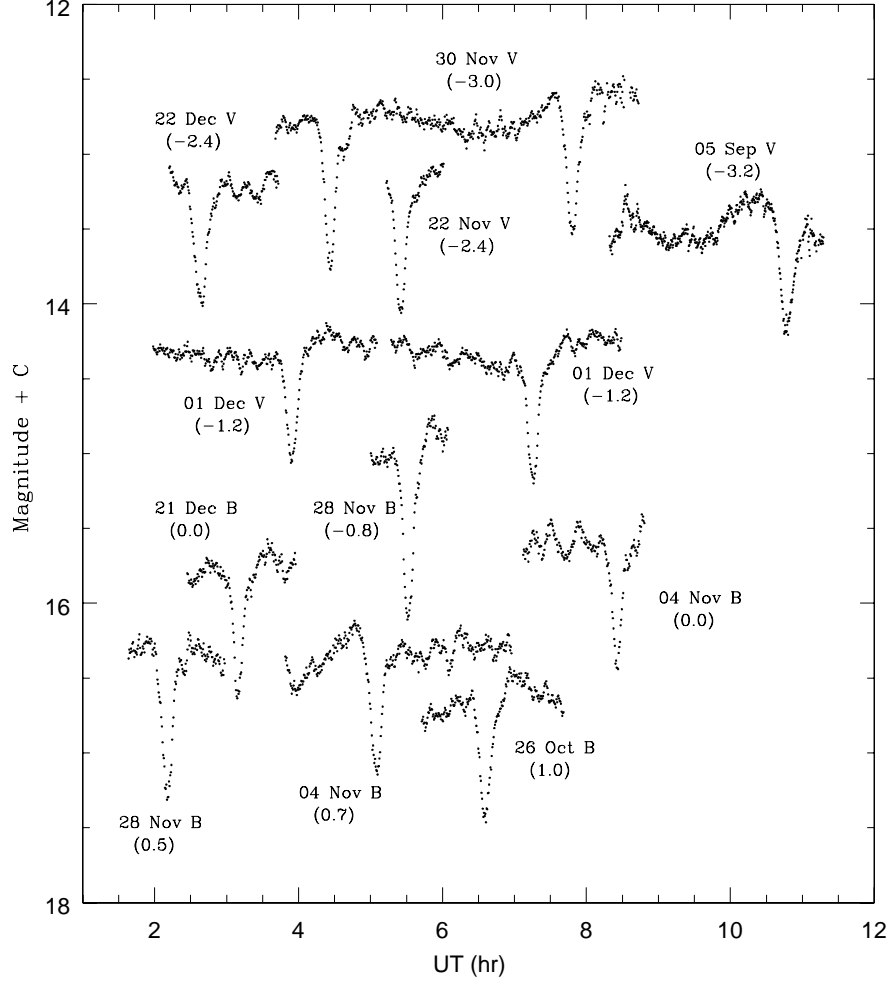


Fig. 1.— The B and V light curves of TT Tri. For clarity of presentation, the data have been offset by addition of the constants given in parentheses under each date.

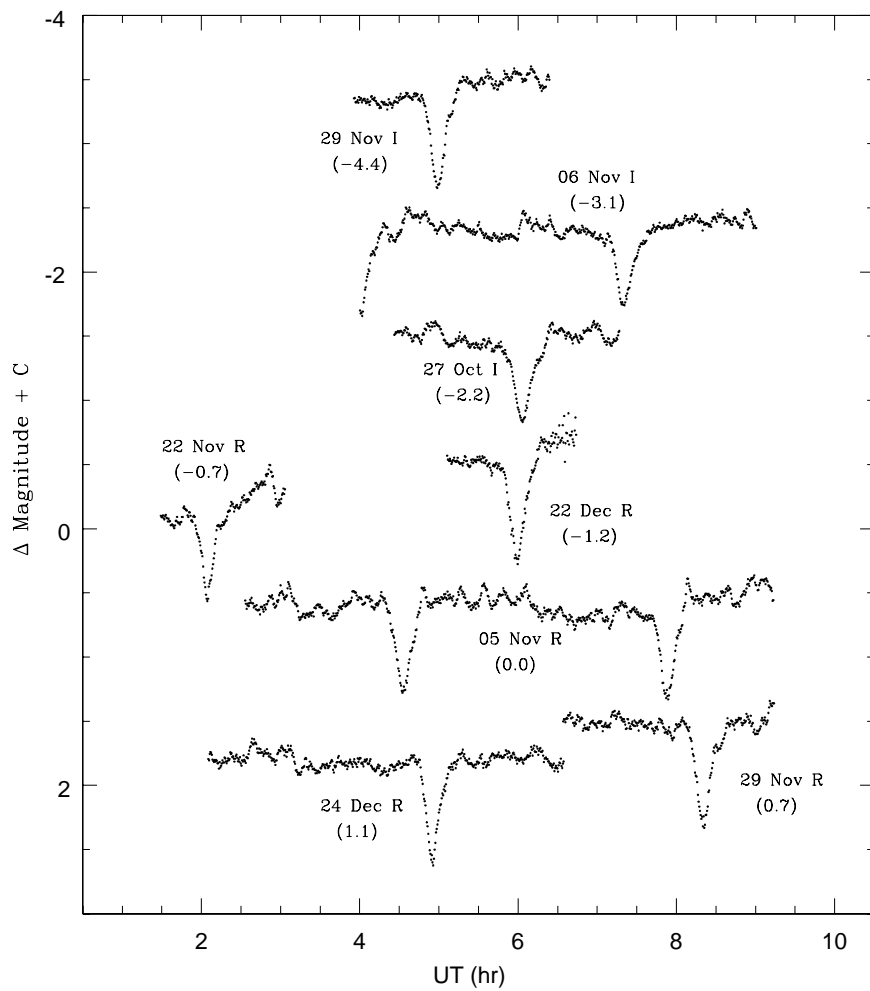


Fig. 2.— The R and I light curves of TT Tri. For clarity of presentation, the data have been offset as in Fig. 1 by addition of the constants given in parentheses under each date.

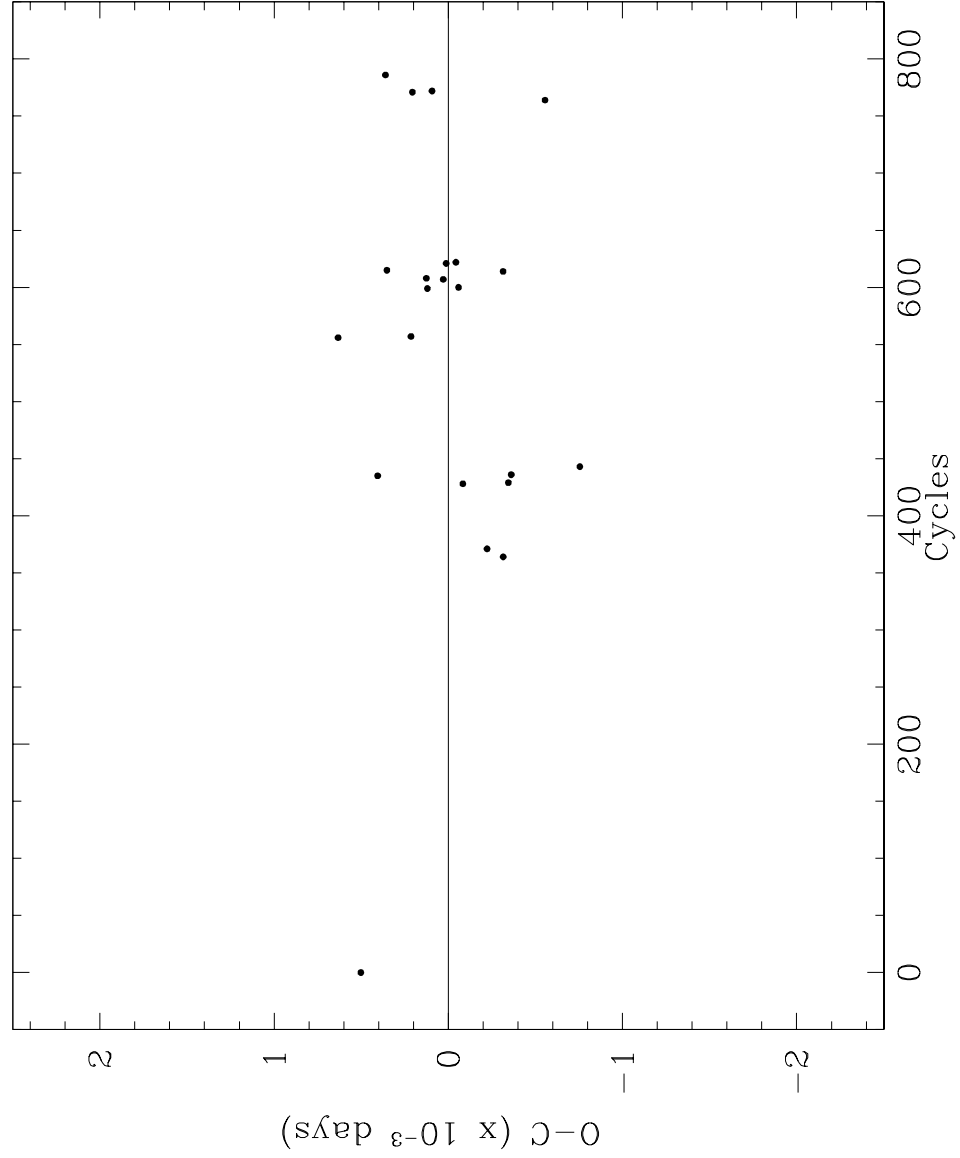


Fig. 3.— The residuals of the the observed times of mid-eclipse with respect to eqn (1) is plotted as a function of cycle number. All timings are within ~ 1 min of those predicted by the ephemeris.

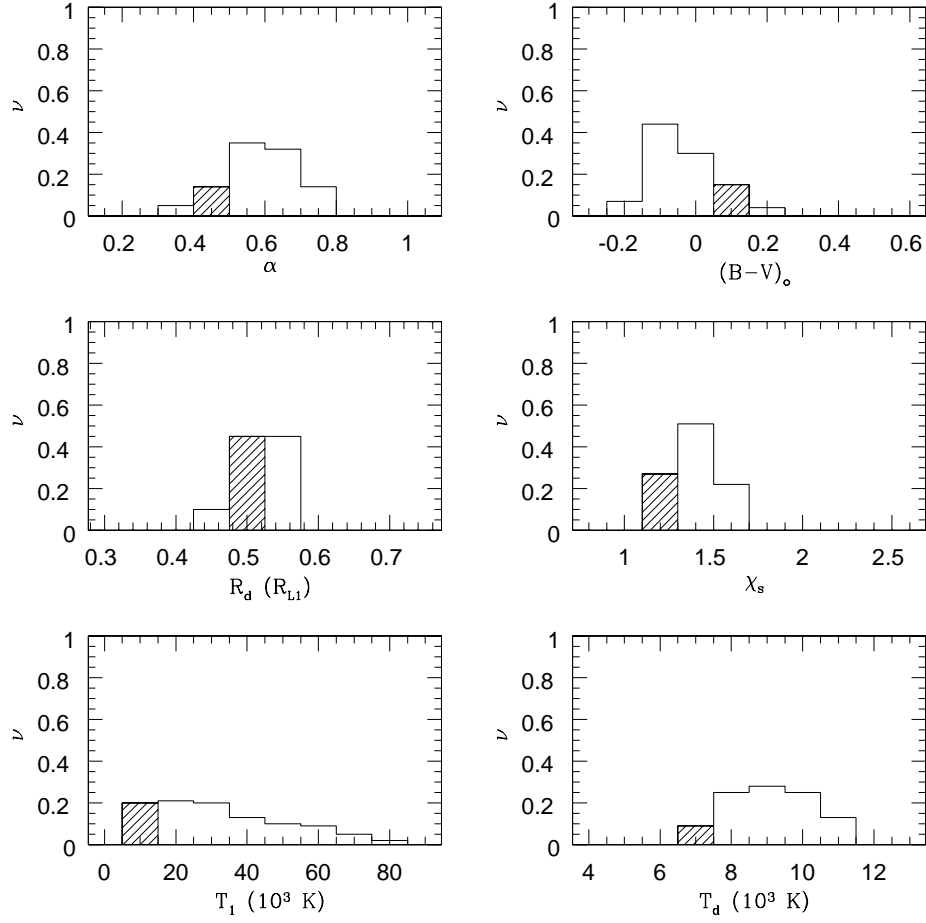


Fig. 4.— The $q = 0.3, h_r = 0.04$ frequency distributions for each fitting parameter. The model $B - V$ value has also been included. The range of each parameter has been chosen to include all combinations of parameters that result in acceptable fits of the top 100 best-fitting models to the data. The cross-hatched regions indicate the parameter values that produce the optimum fit to the data (Table 6).

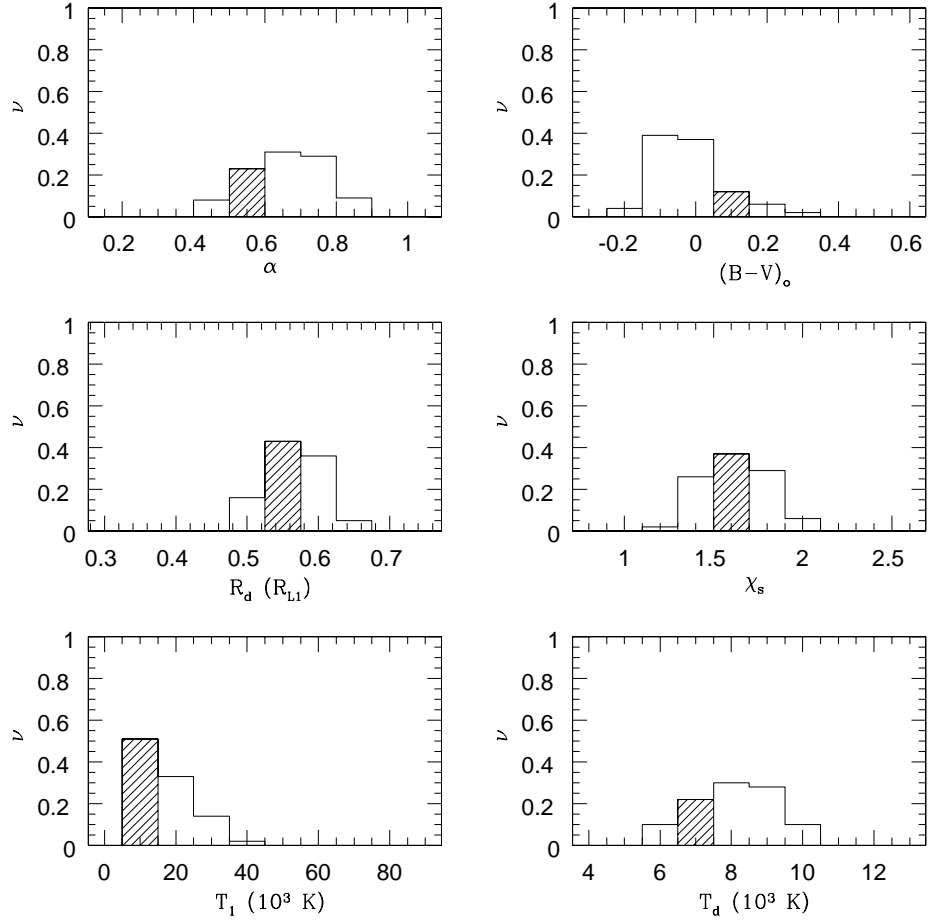


Fig. 5.— The same as Figure 4, but for $q = 0.6$

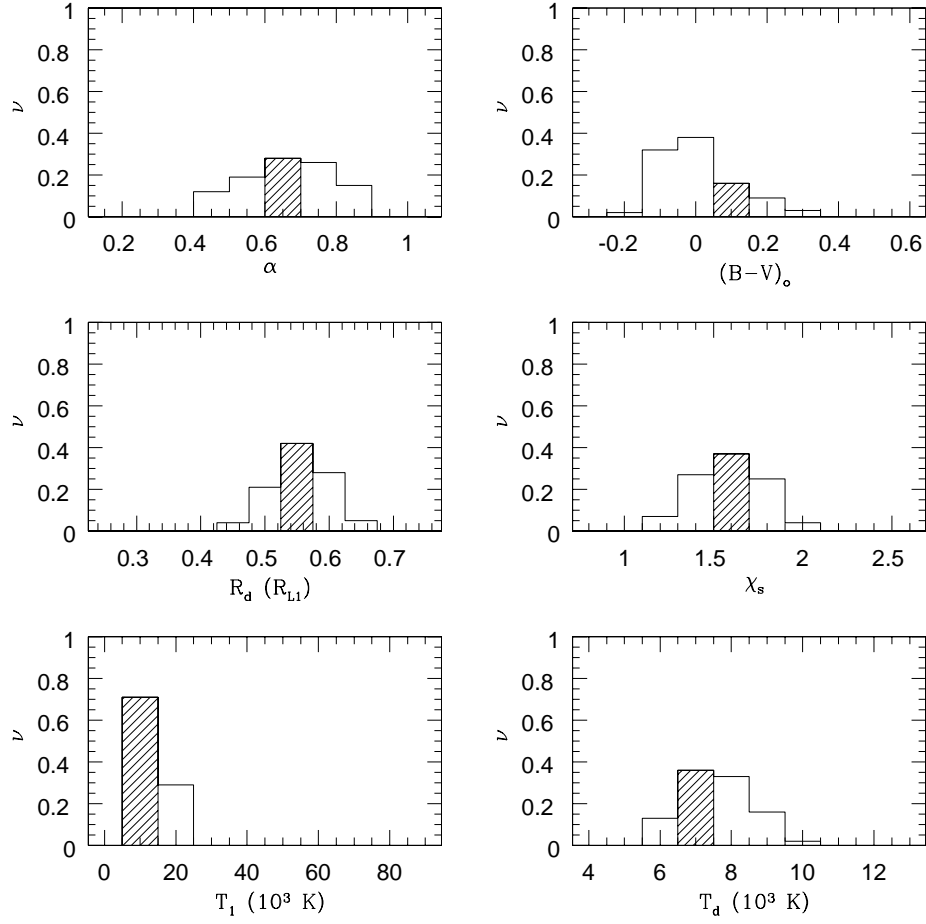


Fig. 6.— The same as Figure 4, but for $q = 0.9$

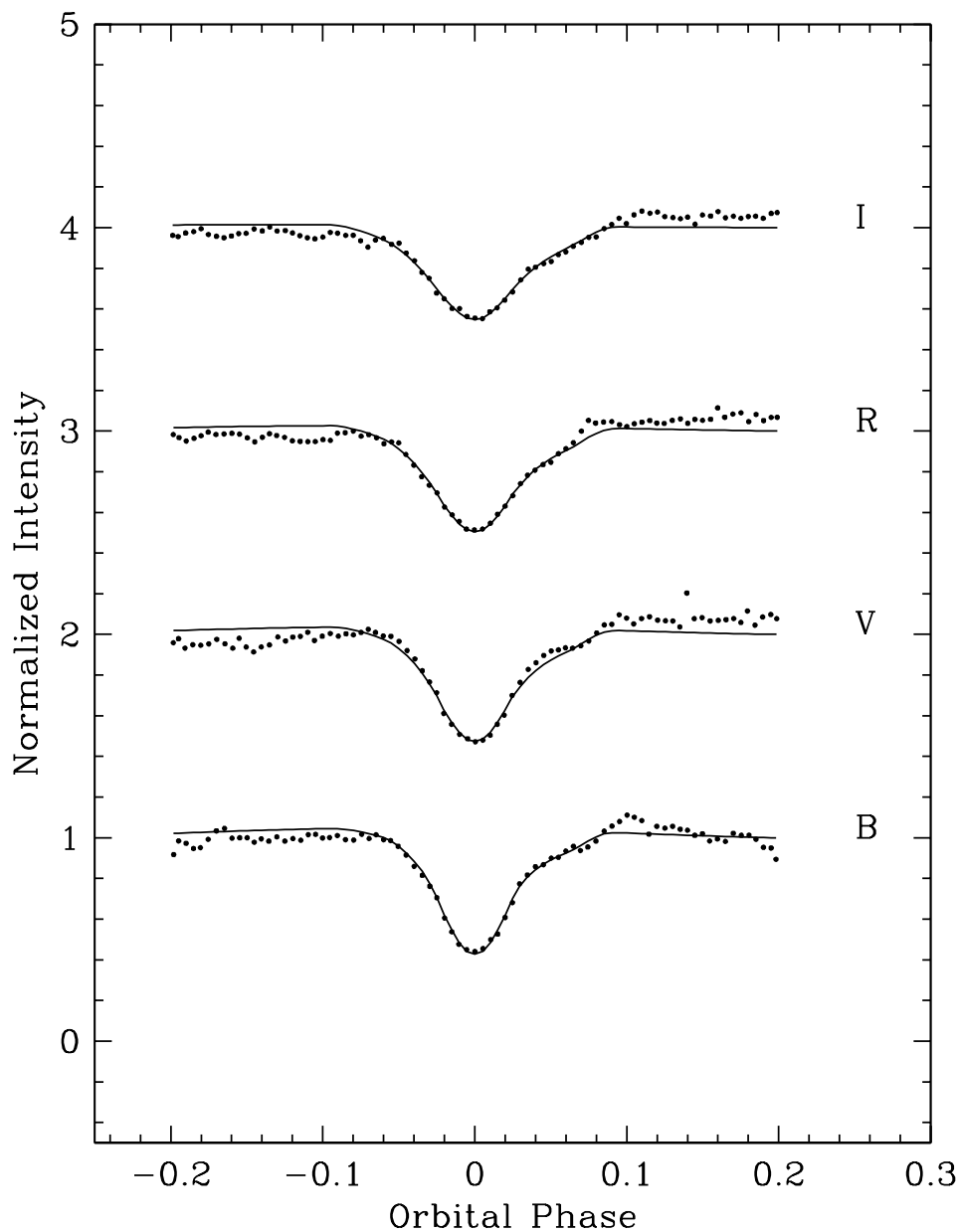


Fig. 7.— The best-fitting eclipse profiles (solid lines) for the $q = 0.6$, $h_r = 0.04$ SD model are plotted together with the observed data. The data have been converted to relative intensity and normalized to unity outside of eclipse, as described in the text. For clarity of presentation the V , R , and I -band light curves and models have been shifted upward by constant offsets of 1, 2, and 3, respectively.

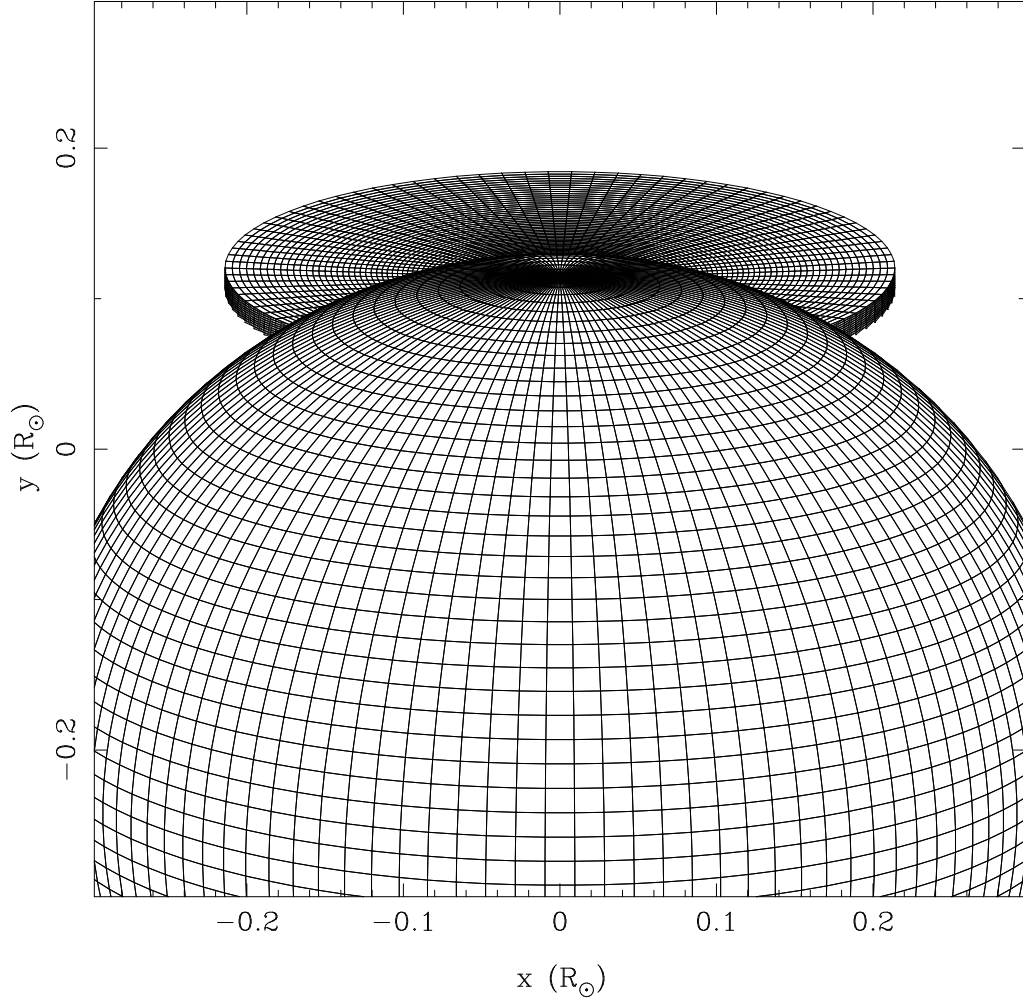


Fig. 8.— A schematic representation of the TT Tri geometry at mid-eclipse for the $q = 0.6, i = 72.6^\circ$ model. Note that the accretion disk is never completely eclipsed, and the white dwarf is barely eclipsed.

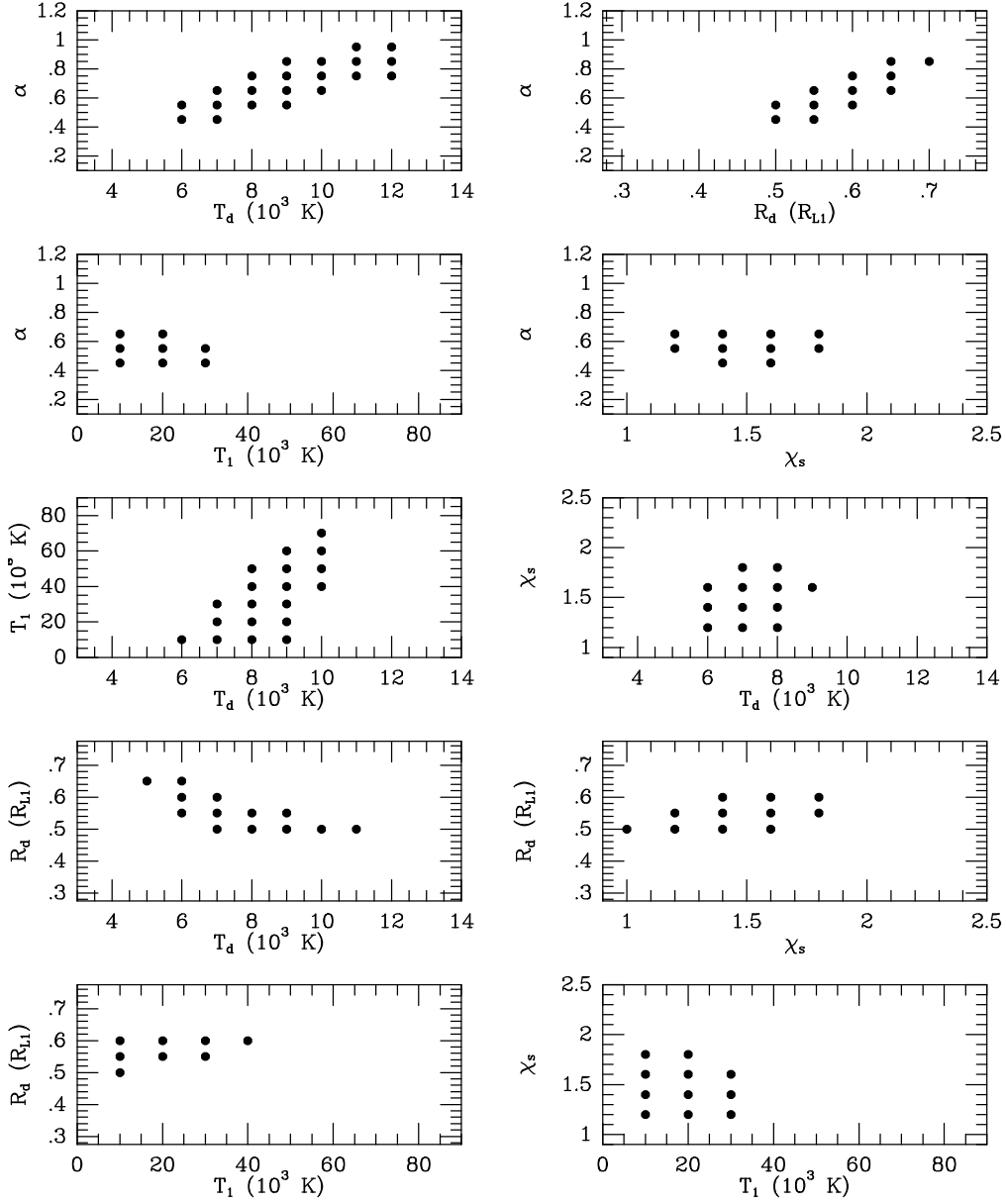


Fig. 9.— The correlations between pairs of model parameters for the $q = 0.6, h_r = 0.04$ SD model are shown for each of the 10 possible pairings of the five fitting parameters. In each case a range of model solutions ($\chi^2_\nu < 2.0$) for each pair of parameters is plotted, while the remaining three parameters are held fixed at their optimum values (Table 6).